

A general end point free energy calculation method based on microscopic configurational space coarse-graining

Kai Wang,[†] Shiyang Long,[†] and Pu Tian^{*,†,‡}

*College of Life Science, and MOE Key Laboratory of Molecular Enzymology and Engineering
Jilin University*

2699 Qianjin Street, Changchun 130012

E-mail: tianpu@jlu.edu.cn

Abstract

Free energy is arguably the most important thermodynamic property for molecular systems. However, current rigorous methodologies for calculating change of which are expensive due to extensive calculations on path(s) connecting end macrostates. Meanwhile, present approximate end-point free energy methods are not sufficiently reliable. Here we develop an alternative end point free energy formulation based on microscopic configurational space coarse graining (misCSCG), where the configurational space of a high dimensional system is divided into a large number of elements, termed conformers. It is shown that when conformers are sufficiently fine and uniform, change of free energy are determined by the number ratio of thermally accessible conformers in end macrostates. Entropy enthalpy compensation arises

*To whom correspondence should be addressed

[†]College of Life Science

[‡]MOE Key Laboratory of Molecular Enzymology and Engineering

Jilin University

2699 Qianjin Street, Changchun 130012

naturally within this theory, and is effectively utilized to avoid calculating strongly fluctuating enthalpic terms in estimating change of free energy. Finally, we demonstrated that misCSCG is feasible by analyzing extensive molecular dynamics simulation trajectories of lipid palmitoleoylphosphatidylcholine.

Introduction

Free energy F of a molecular system is determined by the configurational intergral Z . In canonical ensemble, these two quantities may be described by the following equations:

$$F = -\ln Z \quad (1)$$

$$Z = \sum_m e^{-\beta U_m} \quad (2)$$

with m running through every fundamental (quantum) microstate with potential energy U_m , $\beta = \frac{1}{k_B T}$ is the reciprocal temperature (k_B is Boltzmann constant and T is the temperature). Microstates are well-defined in quantum mechanical description of physical systems. Unfortunately, typical molecular systems in chemical, materials and biological studies, when treated quantum mechanically, present intractable complexity. Classical (continuous) representation of degrees of freedom (DOFs), however, presents an awkward situation for the definition of microstates and entropy.¹ Correspondingly, density of states of classical systems may be determined only up to a multiplicative factor.² Despite the fact that free energy is a state function, a proper integration path, as exemplified by the well-established thermodynamic integration (TI) methodology,^{3,4} needs to be selected to rigorously calculate its difference between end macrostates. Another type of rigorous free energy methods, which are based on non-equilibrium work (NEW) analysis,⁵⁻⁷ require calculation of non-equilibrium work for a large number of paths. All histogram based methods (e.g. weighted histogram analysis method (WHAM)⁸) require an order parameter onto which to map the potential of mean force. Selection of path(s) and/or order parameter(s) in these scenarios is a challenging task in many cases. The free energy perturbation (FEP) approach,⁹⁻¹¹ which

calculates free energy difference directly from sampling the selected reference macrostate, does not need a reaction coordinate. However, the results from single-step FEP is only reliable when two end macrostates have significant overlapping in their respective statistically dominant parts of configurational space, a condition not satisfied in many practical applications. Multi-stage FEP¹² may alleviate this problem, but faces the same challenge of selecting a proper reaction coordinate as in TI. The large amount of computational resources consumed on path(s) connecting end macrostates and unbounded propagation of error^a prevent routine utility of these methods in high throughput applications such as molecular design, docking and folding of biomacromolecules, where it is essential to evaluate free energy differences for a large number of end macrostate pairs. Two presently widely utilized approximate end point free energy methods are linear interaction energy (LIE) model¹³ and MM/P(G)BSA.¹⁴ Unfortunately, reliability of these methods is not satisfactory in many applications due to rough treatments of conformational variation within end macrostates on the one hand, and due to large magnitude of error terms for change of enthalpy and entropy (in comparison with change of free energy) during typical molecular processes on the other hand. A recent development in the field of free energy calculation is hypothetical scanning Monte Carlo (HSMC) and hypothetical scanning molecular dynamics (HSMD) methodologies.^{15–19} These methods directly calculate free energies of end macrostates through reconstruction of probabilities for configurations generated from regular MD or MC procedures. As end point methods, HSMC(D) overcome issues associated with paths and do not have problem of unbounded error propagation when many macrostates are to be evaluated. However, due to the extensive probing of configurational space during calculation of transition probabilities that are essential in reconstruction of probability for each given configuration, HSMC(D) remains significantly more expensive than regular TI calculations for calculating free energy difference between one pair of end macrostates in tested systems.²⁰ In this study, we present an alternative theoretical framework

^aSuppose we have n macrostates $\{MS_1, MS_2, MS_3, \dots, MS_n\}$ to be evaluated for their relative free energy via TI type of methods. If we calculate ΔG^{12} (the free energy change when the system goes from macrostates MS_1 to MS_2), ΔG^{23} , \dots , $\Delta G^{(n-1)n}$, and express ΔG^{1n} as the sum: $\Delta G^{12} + \Delta G^{23} + \dots + \Delta G^{(n-1)n}$, we would have accumulation of error following a one-dimensional random walk, which is not bounded. To prevent such unbounded propagation of error, pairwise calculations are necessary and the resulting number of calculations increase from $\mathcal{O}(n)$ to $\mathcal{O}(n^2)$!

for end point free energy calculation based on microscopic configurational space coarse-graining (misCSCG), where the configurational space of a high dimensional system is divided into a large number of sufficiently fine and uniform elements, termed conformers. It is found that with proper misCSCG, both change of free energy and change of conformational entropy are reliably determined by the number ratio of thermally accessible conformers in end macrostates. Meanwhile, change of average intra-conformer entropy is essentially cancelled by change of enthalpy. Therefore, this formulation provides a fresh perspective to the long standing enigma of entropy-enthalpy compensation, which is taken full advantage to avoid direct calculation of strongly fluctuating change of enthalpy in calculating change of free energy. Using extensive MD trajectories of lipid palmitoylcholine (POPC), we demonstrated feasibility of end point free energy calculation within the misCSCG framework.

The theory of microscopic configurational space coarse graining

As briefed above, classical systems do not have well defined microstates. However, we may artificially define basic states by dividing the full configurational space of a molecular system with a given potential energy function $U(\mathbf{r})$ (with \mathbf{r} being the coordinate vector of all atoms in the system) into $N(U(\mathbf{r}))$ conformers, each is associated with a global probability P_i , such that:

$$Z = \sum_{i=1}^{N(U(\mathbf{r}))} Z_i \quad (3)$$

$$P_i = \frac{Z_i}{Z} \quad (4)$$

$$Z_i = \int_{\Gamma_i} e^{-\beta U(\mathbf{r})} d\mathbf{r} \quad (5)$$

with Γ_i indicating the configurational space corresponding to the i th conformer. For two macrostates A and B that have $N_{conf}^A(U(r))$ and $N_{conf}^B(U(r))$ thermally accessible conformers, denoting their average statistical weight of conformers as w^A and w^B , and the average statistical weight for conformers of the whole configurational space as w , the change of free energy between these two

macrostates may be written, in canonical ensemble, as:

$$\begin{aligned}
\Delta F^{AB} &= k_B T \ln \frac{Z^A}{Z^B} \\
&= k_B T \ln \frac{Z^A/Z}{Z^B/Z} \\
&= k_B T \ln \frac{N_{conf}^A(U(\mathbf{r}))w^A/N(U(\mathbf{r}))w}{N_{conf}^B(U(\mathbf{r}))w^B/N(U(\mathbf{r}))w} \\
&= k_B T \ln \frac{N_{conf}^A(U(\mathbf{r}))}{N_{conf}^B(U(\mathbf{r}))} + k_B T \ln \frac{w^A}{w^B}
\end{aligned} \tag{6}$$

To be concise, we use N , N_{conf}^A and N_{conf}^B instead of $N(U(r))$, $N_{conf}^A(U(r))$ and $N_{conf}^B(U(r))$ hereafter. Apparently, $N_{conf}^A < N$ and $N_{conf}^B < N$.

It is well established in the informational theory field²¹ that for a given static distribution with well-defined basic states, entropy may be constructed by arbitrary division of the whole system into M subparts.

$$S = - \sum_{i=1}^{i=N} P_i \ln P_i = - \sum_{j=1}^{j=M} P_j \ln P_j + \sum_{j=1}^{j=M} P_j S_j \tag{7}$$

$$S_j = - \sum_{k=1}^{k=k_j} P_k \ln P_k \quad (j = 1, 2, \dots, M) \tag{8}$$

$$N = \sum_{j=1}^{j=M} k_j \tag{9}$$

with P_i , P_j and P_k being properly normalized:

$$\sum_{i=1}^{i=N} P_i = 1, \quad \sum_{j=1}^{j=M} P_j = 1 \quad \text{and} \quad \sum_{k=1}^{k=k_j} P_k = 1 \quad (j = 1, 2, \dots, M) \tag{10}$$

S is the global informational entropy and S_j s ($j = 1, 2, \dots, M$) are local informational entropies, it is noted that such division may be carried out recursively. We may similarly construct both local entropies of macrostates (say A and B) and global entropy for the given molecular system based on

a defined set of conformers:

$$S^A = -k_B \sum_{j=1}^{N_{conf}^A} p_j \ln p_j + \sum_{j=1}^{N_{conf}^A} p_j S_j^A \quad (11)$$

$$S^B = -k_B \sum_{k=1}^{N_{conf}^B} q_k \ln q_k + \sum_{k=1}^{N_{conf}^B} q_k S_k^B \quad (12)$$

$$S = -k_B \sum_{i=1}^N P_i \ln P_i + \sum_{i=1}^N P_i S_i \quad (13)$$

P_i is the probability of the i th conformer in the global configurational space, $p(q)_{j(k)}$ is the probability of the $j(k)$ th conformer in macrostate $A(B)$. S_i is the intra-conformer entropy of the i th conformer in the global configurational space. $S_{j(k)}^{A(B)}$ is the intra-conformer entropy for the $j(k)$ th conformer in macrostate $A(B)$. Again, P_i , p_j and q_k are properly normalized:

$$\sum_{i=1}^N P_i = 1, \quad \sum_{j=1}^{N_{conf}^A} p_j = 1 \quad \text{and} \quad \sum_{k=1}^{N_{conf}^B} q_k = 1 \quad (14)$$

The first terms on the right hand side of equations (Eq. (11), Eq. (12) and Eq. (13)) describe distributions of conformers within a macrostate or within the whole configurational space, and is referred to as “conformational entropy” (S_{conf}), the second terms are averages of the intra-conformer entropies of corresponding conformers and are denoted $\overline{S_{int}}$. We may rewrite S^A and S^B in the following form:

$$S^A = S_{conf}^A + \overline{S_{int}^A} \quad (15)$$

$$S_{conf}^A = -k_B \sum_{j=1}^{N_{conf}^A} p_j \ln p_j \quad (16)$$

$$\overline{S_{int}^A} = \sum_{j=1}^{N_{conf}^A} p_j S_j^A \quad (17)$$

$$S^B = S_{conf}^B + \overline{S_{int}^B} \quad (18)$$

$$S_{conf}^B = -k_B \sum_{k=1}^{N_{conf}^B} q_k \ln q_k \quad (19)$$

$$\overline{S_{int}^B} = \sum_{k=1}^{N_{conf}^B} q_k S_k^A \quad (20)$$

With a simple algebraic manipulation shown below:

$$\begin{aligned} S_{conf}^A &= -k_B \sum_{j=1}^{N_A} p_j \left(\ln p_j - \ln N_{conf}^A + \ln N_{conf}^A \right) \\ &= k_B \ln N_{conf}^A - k_B \sum_{j=1}^{N_{conf}^A} p_j \ln N_{conf}^A p_j \end{aligned} \quad (21)$$

Conformational entropy of macrostate A (S_{conf}^A) is divided into two terms. The first term is the Boltzmann entropy (or ideal gas entropy, denoted as $S_{Boltzmann}^A$) based on the number of conformers. The second term represents deviation from the Boltzmann entropy (denoted as δS_{conf}^A). It is the product of the Boltzmann constant and the Kullback-Leibler divergence²² between the actual probability distribution of conformers in macrostate A ($\mathbf{p} = (p_1, p_2, \dots, p_{N_{conf}^A})$) and the uniform distribution ($unif\{1, N_{conf}^A\}$). S_{conf}^A may be rewritten as:

$$S_{conf}^A = S_{Boltzmann}^A + \delta S_{conf}^A \quad (22)$$

$$\delta S_{conf}^A = -k_B D_{KL}(\mathbf{p} || unif\{1, N_{conf}^A\}) \quad (23)$$

Note that $D_{KL}(\mathbf{p} || unif\{1, N_{conf}^A\}) \geq 0$. Using mathematical relation $\ln x \leq x - 1$ (for $x > 0$):

$$\begin{aligned} |\delta S_{conf}^A| &\leq k_B \sum_{j=1}^{N_{conf}^A} p_j (N_{conf}^A p_j - 1) \\ &= k_B \left(N_{conf}^A \sum_{j=1}^{N_{conf}^A} p_j^2 - 1 \right) \end{aligned} \quad (24)$$

Given the normalization constraints $\sum_{j=1}^{N_{conf}^A} p_j = 1$, let $\delta_j = \frac{1}{N_{conf}^A} - p_j$, It is easily shown that $N_{conf}^A \sum_{j=1}^{N_{conf}^A} p_j^2 = 1 + N_{conf}^A \sum_{j=1}^{N_{conf}^A} \delta_j^2$, therefore,

$$|\delta S_{conf}^A| \leq N_{conf}^A \sum_{j=1}^{N_{conf}^A} \delta_j^2 \quad (25)$$

Note that the square of standard deviation of \mathbf{p} $\sigma_p^2 = \frac{\sum_{j=1}^{N_{conf}^A} \delta_j^2}{N_{conf}^A}$. Therefore, we have:

$$|\delta S_{conf}^A| \leq k_B N_{conf}^A \sigma_p^2 \quad (26)$$

Similarly, denote probability distribution of conformers in macrostate B as $\mathbf{q} = (q_1, q_2, \dots, q_{N_{conf}^B})$ and the corresponding uniform distribution as $unif\{1, N_{conf}^B\}$, we have:

$$S_{conf}^B = S_{Boltzmann}^B + \delta S_{conf}^B \quad (27)$$

$$\delta S_{conf}^B = -k_B D_{KL}(\mathbf{q} || unif\{1, N_{conf}^B\}) \quad (28)$$

and

$$\begin{aligned} |\delta S_{conf}^B| &\leq k_B \sum_{k=1}^{N_{conf}^B} q_k (N_{conf}^B q_k - 1) \\ &= k_B N_{conf}^B \sigma_q^2 \end{aligned} \quad (29)$$

In reality, we rarely care the absolute entropy or free energy of a specific system. Instead, what we are most interested in is the change of these quantities between our interested macrostates of a given molecular system. Again, using the above mentioned macrostates A and B as the example:

$$\begin{aligned} \Delta F^{AB} &= \Delta U^{AB} - T \Delta S^{AB} \\ &= \Delta U^{AB} - T \left(S_{conf}^B + \overline{S_{int}^B} - S_{conf}^A - \overline{S_{int}^A} \right) \end{aligned} \quad (30)$$

ΔU^{AB} is the change of potential energy between the two macrostates A and B . Let:

$$\delta F^A = -k_B T \ln \frac{w_A}{w} \quad (31)$$

$$\delta F^B = -k_B T \ln \frac{w_B}{w} \quad (32)$$

$$\Delta \delta F^{AB} = k_B T \ln \frac{w_A}{w_B} \quad (33)$$

$$\Delta S_{int}^{AB} = \overline{S_{int}^B} - \overline{S_{int}^A} \quad (34)$$

$$\Delta S_{conf}^{AB} = S_{conf}^B - S_{conf}^A \quad (35)$$

$$\Delta \delta S_{conf}^{AB} = \delta S_{conf}^B - \delta S_{conf}^A \quad (36)$$

we have:

$$\Delta F^{AB} = k_B T \ln \frac{N_{conf}^A}{N_{conf}^B} + \Delta \delta F^{AB} = \Delta F_{Boltzmann}^{AB} + \Delta \delta F^{AB} \quad (37)$$

$$\Delta S_{conf}^{AB} = -k_B \ln \frac{N_{conf}^A}{N_{conf}^B} + \Delta \delta S_{conf}^{AB} = \Delta S_{Boltzmann}^{AB} + \Delta \delta S_{conf}^{AB} \quad (38)$$

$$\Delta U^{AB} = T \Delta S_{int}^{AB} + \Delta \delta F^{AB} + T \Delta \delta S_{conf}^{AB} \quad (39)$$

When conformers are sufficiently uniform, $\Delta \delta F^{AB} \approx 0$, upper bounds for the absolute value of both δS_{conf}^A and δS_{conf}^B , which are $k_B N_{conf}^A \sigma_p^2$ and $k_B N_{conf}^B \sigma_q^2$, are on the order of unity or smaller. More importantly, the subtraction causes effective error cancellation. Therefore, we have $\Delta \delta S_{conf}^{AB} \approx 0$. These conditions will result in the following approximations:

$$\Delta F^{AB} \approx \Delta F_{Boltzmann}^{AB} \quad (40)$$

$$\Delta S_{conf}^{AB} \approx \Delta S_{Boltzmann}^{AB} \quad (41)$$

$$\Delta U^{AB} \approx T \Delta S_{int}^{AB} \quad (42)$$

While our derivation is carried out in canonical ensemble, it should be applicable for many isobaric-isothermal processes (e.g. many biomolecular systems under physiological conditions or rou-

tine experimental conditions) where change of PV term is negligible. Equations (Eq. (40)) and (Eq. (41)) indicate that when proper misCSCG is carried out, conformers exhibit approximate ideal gas behavior. It is certainly a desirable property as figuring out exact probability for each conformer is an expensive and necessary task in brute force calculation/estimation of partition function. One immediately arising question is how to define sufficiently uniform conformers, if it is ever possible, for a given complex molecular system? In this study we use extensive MD simulation trajectories of lipid POPC to validate that equations (Eq. (40)) and (Eq. (41)) based on misCSCG are feasible ways for end point free energy and conformational entropy calculations.

Analysis of MD trajectories

Test strategy

Equations (Eq. (37), Eq. (38) and Eq. (39)) are exact regardless of specific conformer definitions. The reason we used the term “microscopic” is that for any high dimensional complex molecular systems that are meaningfully characterizable experimentally (e.g. structure of a well-folded protein or predictable behavior of an inherently disordered protein), statistical weights of macroscopic conformers have to be exponentially different so that we may make reliable observations despite their enormous sizes of configurational space. The powerful nested sampling²³ strategy is based on this very fact, which results in domination of $\Delta\delta$ terms over the Boltzmann terms in equations (Eq. (37)) and (Eq. (38)). Consequently, approximations in equations (Eq. (40)), (Eq. (41)) and (Eq. (39)) break down. Therefore, “microscopic” (or sufficiently fine) partitioning of configurational space is essential to achieve desired uniformity of conformers. With microscopic definition of conformers, the absolute values of corresponding conformational entropy S_{conf} for typical complex molecular systems (e.g. proteins, nucleic acids, lipids or polysaccharides) are extremely difficult, if ever possible, to be obtained by a direct sampling approach. In regular MD simulations, one rarely record more than a billion snapshots. In regular biochemical experiments, usually nanomolar or much less solutes are used. The allowed number of combinations of side chain rotameric

states for 76-residue ubiquitin, with its backbone configuration fixed in the the crystal structural state with PDB code *1ubq*, is estimated to be as many as $\sim 10^{40}$ (unpublished data) based on a rigid rotamer model.²⁴ Therefore, direct analysis of conformational entropy is an intractable problem, and is inaccessible from either regular MD trajectories or routine experiments. In reality, the measured change of conformational entropy for a typical major conformational change between two macrostates *A* and *B* is the converged change of observed local conformational entropies.

$$\Delta S_{conf}^{AB} = \Delta S_{conf}^{O-AB} = S_{conf}^{O-A} - S_{conf}^{O-B} \quad (43)$$

with *O*– indicating observed part of the specified configurational space defining a macrostate. The observed local conformational entropy and corresponding approximate Boltzmann entropy may be, following equations (Eq. (21)) and (Eq. (22)), written as:

$$\begin{aligned} S_{conf}^{O-A} &= -k_B \sum_{i=1}^{N_{conf}^{O-A}} p_i^{O-} \ln p_i^{O-} \\ &= S_{Boltzmann}^{O-A} + \delta S_{conf}^{O-A} \end{aligned} \quad (44)$$

$$S_{Boltzmann}^{O-A} = k_B \ln N_{conf}^{O-A} \quad (45)$$

$$\delta S_{conf}^{O-A} = -k_B D_{KL}(\mathbf{p}^{O-} || \text{unif}\{1, N_{conf}^{O-A}\}) \quad (46)$$

with N_{conf}^{O-A} being the number of observed conformers in *A*, and $\mathbf{p}^{O-} = (p_1^{O-}, p_2^{O-}, \dots, p_{N_{conf}^{O-A}}^{O-})$ being the observed probabilities of conformers. Correspondingly, the observed free energy difference between two given part of configurational space may be effectively calculated based upon observed probabilities.

$$\Delta F^{AB} = \Delta F^{O-AB} = k_B T \ln \frac{P^{O-A}}{P^{O-B}} \quad (47)$$

with *A* and *B* being two arbitrarily given macrostates, P^{O-A} and P^{O-B} being observed probabilities (or relative populations), which are effectively represented by the number of observed snapshots (N_{snap}^{O-A} and N_{snap}^{O-B}) in equilibrium MD trajectories. Imagining that there is a reference macrostate

in equilibrium with other visited parts of configurational space, and this macrostate has a statistical weight corresponding to 1 snapshot, then observed relative free energy of any given macrostate A with respect to this reference state may be written as:

$$F^{O-A} = -k_B T \ln N_{snap}^{O-A} \quad (48)$$

Similarly, for a given macrostate A with N_{conf}^{O-A} conformers, we may write its approximate relative free energy based on conformer count as:

$$F_{Boltzmann}^{O-A} = -k_B T \ln N_{conf}^{O-A} \quad (49)$$

with an imagined reference state holding 1 conformer. For initial validation of equations (Eq. (40)) and (Eq. (41)), direct comparison with free energy change from well-established experimental measurement (e.g. isothermal calorimetry (ITC)²⁵), while highly desirable, is not straight forward. The reason is that to effectively compare with experimental values, we need to deconvolute force fields and sampling errors from fundamental deficiencies of the method, which is a challenge to be met and an issue beyond the scope of this study. Meanwhile, direct comparison with population based free energy and corresponding conformational entropy change (equations Eq. (48) and Eq. (44)) derived from MD trajectories at least removes convolution of force field deficiency. In this study, to effectively utilize MD trajectory sets for testing robustness of the end point free energy method as embodied in equations (Eq. (40)) and (Eq. (41)), we adopted the following two strategies:

Firstly, MD trajectories provide a convenient path for arbitrary partitioning of configurational space, and for examining change of both free energy and conformational entropy between any given pair of observed macrostates. For a given molecular system with specific definition of conformers, validity of equations (Eq. (40)) and (Eq. (41)) requires that both S_{conf}^{O-} vs. $S_{Boltzmann}^{O-}$ and F^{O-} vs. $F_{Boltzmann}^{O-}$ plots exhibit perfect linear correlation (i.e. with linear correlation coefficients approaching unity) with a unity slope. The accuracy of equations (Eq. (40)) and (Eq. (41)) would

be reflected by both slopes and linear correlation coefficients of these two types of plots, while their precision would be reflected by the extent of deviations from injection (i.e. spreading of data points away from single valued lines) in these plots. Conversely, based on the logic that *rule of conformer distribution manifested among arbitrarily selected parts of configurational space should be effectively true for the whole configurational space*, observed near-unity slopes and linear correlation coefficients in these two types of plots directly support the validity of equations (Eq. (40)) and (Eq. (41)). It is important to note that such validity is inherently limited by finite and small configurational space visited by MD trajectories.

Secondly, since the population based free energy differences derived from MD simulation trajectories are limited by their collective time scale (CTS). Therefore, with increasing volume of visited configurational space by larger trajectory sets, it is essential for $\Delta\delta$ terms in equations (Eq. (37)) and (Eq. (38)) to exhibit a non-increasing trend for the inferred validity of equations (Eq. (40)) and (Eq. (41)) in macroscopic MD simulations (e.g. trajectories with CTS comparable with relevant experimental characterizations). It is important to note that observations from thought macroscopic MD simulations would likely be different from an experimental measurement under the same condition, with the extent of differences determined by the quality of force fields. To overcome the limitation of finite sampling that is inherent in MD trajectories, we calculated both distributions of $\Delta\delta$ terms in equations (Eq. (37)) and (Eq. (38)) and cumulative probability density (CPD) of their absolute values for trajectory sets with various sizes and analyzed their trend of change.

Analysis of POPC trajectories

Definition of trajectory sets, conformers and macrostates

Lipids are important biomolecules that are major components of cell membranes. Since misCSCG is a general theoretical framework for high dimensional complex systems, we figure it should be applicable for lipid POPC, for which large MD trajectory sets are available. To carry out testing of approximate free energy and conformational entropy equations (Eq. (40) and Eq. (41)), we firstly

extracted MD trajectories of POPC from trajectories of M2 muscarinic acetylcholine receptor.²⁶ Three increasingly larger trajectory sets, TSA1, TSA2 and TSA3 were constructed with smaller trajectory sets being subsets of larger ones. Secondly, we defined four different sets of conformers, which were denoted as CONF1 through CONF4 (see Fig. Figure 1) respectively, with CONF1 being the finest and CONF4 being the coarsest. Thirdly, we used backbone dihedrals as order parameters to construct macrostates. Finally, number of conformers (N_{conf}) were calculated for each macrostate of the given trajectory set and definition of conformers. See *Methods* for details.

Results

For each macrostate j (j runs through all constructed macrostates) within a given combination of trajectory set and definition of conformers, we calculated observed population based local relative free energy F^{O-j} (equation (Eq. (48))), observed conformer count based local relative free energy $F_{Boltzmann}^{O-j}$ (equation (Eq. (49))), observed local conformational entropy S_{conf}^{O-j} (equation (Eq. (44))) and observed local Boltzmann entropy based on conformer count $S_{Boltzmann}^{O-j}$ (equation (Eq. (45))). For each of the total 12 combinations of trajectory sets and conformers, F^{O-j} vs. $F_{Boltzmann}^{O-j}$ (termed as *free energy plot* hereafter) and S_{conf}^{O-j} vs. $S_{Boltzmann}^{O-j}$ (termed as *conformational entropy plot* hereafter) plots were constructed and shown in Fig. (Figure 2) and Fig. (Figure 3).

For CONF1 and CONF2, regardless of size of trajectory set, near perfect accuracy and precision were observed for both *free energy plots* (Fig. Figure 2a-f) and *conformational entropy plots* (Fig. Figure 3a-f), with both slopes and squared linear correlation coefficients approaching unity, and all data points falling on straight data-fitting lines (green), which are essentially not distinguishable from blue lines that represent equation (Eq. (40)) in *free energy plots* (or equation (Eq. (41)) in *conformational entropy plots*). For CONF3, while good accuracy and precision is observed for the smallest trajectory set TSA1 (Fig. Figure 2g and Fig. Figure 3g), deterioration of both accuracy and precision were observed for larger trajectory sets (Fig. Figure 2h-i and Fig. Figure 3h-i). For CONF4, the coarsest conformers tested, significantly deteriorated accuracy and precision were observed (Fig. Figure 2j-l and Fig. Figure 3j-l). For both CONF3 and CONF4,

deterioration of accuracy and precision for conformer-count based free energy and conformational entropy (equations Eq. (40) and Eq. (41)) occurs mainly for relatively heavier macrostates (lower-left part in *free energy plots* and upper-right part in *conformational entropy plots*), with the extent of deterioration for both accuracy and precision increases with increasing size of trajectory set.

The distributions of $\Delta\delta F$ and CPD of its absolute values for the four defined conformers (CONF1 through CONF4) are shown in two left columns in Fig. Figure 4a-h. Correspondingly, distributions of $\Delta\delta S_{conf}$ and CPD of its absolute values are shown in two right columns in Fig. Figure 4i-p. As one would intuitively expecting, both $\Delta\delta F$ and $\Delta\delta S_{conf}$ exhibit single peak distribution with the mode being approximately zero. With increasing conformer coarseness, the range of $\Delta\delta F$ increases significantly from a few percent of $k_B T$ (CONF1, Fig. Figure 4a,e) to a few $k_B T$ (CONF4, Fig. Figure 4d,h). $\Delta\delta S_{conf}$ shows the same trend. For CONF1 (Fig. Figure 4a,i), both $\Delta\delta$ terms show broader distributions with smaller trajectory set, a qualitatively different trend from other three CONFs (CONF2, CONF3 and CONF4, rows 2 through 4 in Fig. Figure 4), where both $\Delta\delta$ terms show broader distributions with larger trajectory set. Such difference may be seen better in CPD plots (Fig. Figure 4e-h and Fig. Figure 4m-p). As discussed in section *Test strategy*, due to limited sampling in MD trajectories, to extend validity of equations (Eq. (40)) and (Eq. (41)) supported by observed accuracy and precision in *free energy* and *conformational entropy plots* based on regular MD trajectories to macroscopic observations, a non-increasing trend for $\Delta\delta$ terms with increasing size of visited configuration space is essential. Therefore, we conclude that for POPC, only CONF1s are sufficiently fine and uniform conformers, whose count may be effectively utilized to predict free energy change between arbitrarily specified macrostates. However, CONF2 is manifested as a good candidate for microscopically coarse graining POPC configurational space as far as accuracy and precision in *free energy plots* (Fig. Figure 2d-f) and *conformational entropy plots* (Fig. Figure 3d-f) are concerned. These results suggest that observation of good accuracy and precision in both *free energy* and *conformational entropy plots* is only a necessary condition for validity of equations (Eq. (40)) and (Eq. (41)), especially when data set is small. The limita-

tion of finite sampling in MD trajectories is clearly reflected in the smallest trajectory set TSA1 (with CTS of $\sim 143\mu s$), where good accuracy and precision is observed for CONF3 in both *free energy* (Fig. Figure 2g) and *conformational entropy plots* (Fig. Figure 3g), while significant deterioration of accuracy and precision is manifested in the largest trajectory set (Fig. Figure 2i and Fig. Figure 3i). The increase of absolute values for $\Delta\delta$ terms with increasing size of trajectory set for coarse conformers is expected, as the heterogeneity of conformer statistical weight for coarse conformers is not sufficiently manifested in small trajectory set. Correspondingly, the decrease of absolute values for $\Delta\delta$ terms with increasing size of trajectory set for sufficiently fine and uniform conformers is expected as well, the underlying mechanism is that increasing statistics improves error cancellations. To test the robustness of these two observed trends, we analyzed many different combinations of trajectory sets, which are similar to the trio TSA1, TSA2 and TSA3 with smaller set being subsets of larger ones, and similar trends were observed. A representative figure is presented for a group of trajectory set combinations in Fig. Figure 5. For CONF1 (Fig. Figure 5a,e), some variations are observed across different equally-sized trajectory sets (six smallest trajectory sets TSB1a through TSB1f are shown in red lines; five intermediate trajectory sets TSB2a through TSB2e are shown in green lines), but the trend of decreasing absolute values of $\Delta\delta$ terms with increasing trajectory set size remain unchanged. For CONF2 through CONF4 (Fig. Figure 5b-d, f-h), corresponding small trajectory sets manifest negligible differences and lines in the same color (red lines and green lines) completely overlap, with the trend of increasing absolute values of $\Delta\delta$ terms with increasing trajectory set size clearly observed.

Discussion

Entropy enthalpy compensation

It is important to note that equation Eq. (42) is essentially the intriguing entropy-enthalpy compensation (EEC) phenomena (when PV term is negligible), which had long been an enigma,^{27–31} and has attracted a revival of interest due to its critical relevance in protein-ligand interactions.^{32–44}

Careful statistical analysis confirm that EEC does exist to various extent in many protein-ligand interaction systems after experimental errors are effectively removed.³⁸ A recent hidden factor analysis associate EEC to a Carnot-cycle model where an effective micro-phase transition is shown to be critical.^{35,40} Ahmad *et. al.*⁴⁴ performed a perturbation-based theoretical treatment of EEC, their derivation demonstrated that intrinsic changes of enthalpy and entropy upon a conformational change cancel each other exactly, which suggests that in addition to widely believed solvent reorganization,²⁷ solutes also contribute to EEC. Such analyses, while being insightful for mechanistic understanding of the underlying molecular process, do not provide a path for effective utilization of EEC in rapid and efficient calculation of change of free energy, the quantity of the ultimate interest. EEC arises naturally within our misCSCG framework as a universal property of high dimensional complex molecular systems. For a given molecular system, once we have a well designed misCSCG strategy so that $\Delta\delta$ terms in equations (Eq. (37)) and (Eq. (38)) approach vanishing, equations (Eq. (40)) and (Eq. (42)) state that if the change of molecular interactions does not significantly change the number of available conformers, the free energy of the molecular system will not change considerably. The remaining effect from change of molecular interactions will be cancelled almost completely by corresponding change of average intra-conformer entropy. Note that correlation of neither signs nor magnitudes between ΔS_{conf}^{AB} and ΔS_{int}^{AB} is implied. Therefore, depending upon signs and magnitudes of ΔS_{conf}^{AB} and ΔU (we neglect PV term here), this theory is compatible with various extent of net observed EEC. When $\Delta S_{conf}^{AB} \approx 0$, perfect EEC would be observed; when $\Delta S_{conf}^{AB} > 0$ and $\Delta U > 0$ (or $\Delta S_{int}^{AB} > 0$), a seemingly entropy driven (and a reverse entropy limited) process would be observed; when $\Delta S_{conf}^{AB} > 0$ and $\Delta U < 0$ (or $\Delta S_{int}^{AB} < 0$), depending upon the sign of ΔS , a seemingly enthalpy or entropy-enthalpy jointly driven (and a reverse enthalpy or entropy-enthalpy jointly limited) process would be observed. The fundamental new perspective provided by equation (Eq. (42)) is that EEC is directly related to local redistribution of microstates in configurational space, while change of free energy and conformational entropy reflect the collective thermal accessibility of the global configurational space. Based on the widespread observation of strong EEC effect in many molecular systems, it was suggested⁴¹

that any attempt to calculate the change of free energy as a sum of its enthalpic and entropic contributions is likely to be unreliable. In addition to the rough treatment of conformational variation within end macrostates, both presently widely utilized end point free energy methods, LIE¹³ and MM/P(G)BSA,¹⁴ directly calculate strongly fluctuating enthalpy change. The HSMC(D) methodologies, while being rigorous on conformational variation within end macrostates, involve explicit calculation of exact probabilities for selected configurations, and consequently directly utilizing the strongly fluctuating enthalpic component. By designing a proper misCSCG scheme, EEC is utilized nearly to its full potential in equations (Eq. (40), Eq. (41) and Eq. (42)) by separating a component of change of free energy, the change of conformational entropy, which is approximately equal to the change of free energy with a mere difference of negative temperature factor, from strongly fluctuating change of average intra-conformer entropy that effectively cancels change of enthalpy. Therefore, the methodology should at least in principle be an easily converging methodology with a theoretical superiority to other methods involving direct evaluation of strongly fluctuating quantities, change of enthalpy and/or change of total entropy. Additionally, our formulation gives explicit error ($\Delta\delta$) terms for both change of free energy and change of conformational entropy. Since $\Delta\delta$ terms are local properties of end macrostates, they may be evaluated through local sampling to assess a given misCSCG strategy.

Extremes of misCSCG

The microscopic extreme of misCSCG is that there is no coarse graining at all, with each quantum state being explicitly considered as a conformer. The other is the macroscopic extreme where the whole configurational space of a molecular system is defined as a conformer. For the microscopic extreme of misCSCG, intra-conformer entropy becomes zero as there is no uncertainty for the molecular system once we know that it is in a specific quantum state. For the macroscopic extreme, the conformational entropy becomes zero. Apparently, these two scenarios are trivially equivalent except the fact that the total entropy is termed as conformational entropy for the former case and intra-conformer entropy for the latter case, and we return to where we start. Approaching

the microscopic extreme, the number of conformers is likely to drastically increase and the task of counting them may become difficult or even unpractical. Meanwhile, the number of fundamental quantum states within each conformer decreases accordingly, and distribution of relative statistical weight for conformers will likely to broaden and $\Delta\delta$ terms increase in value correspondingly. Approaching the macroscopic extreme, the conformers are so large and few that the conformational entropy is negligible while intra-conformer entropy takes the central position. As discussed in *Test strategy* section, macroscopic partitions have exponentially different statistical weight. This is evidenced by significant increase of $\Delta\delta$ terms for coarser and coarser definition of conformers for lipid POPC (Fig. Figure 4). Consistently, in *free energy* and *conformational entropy plots* of POPC (Fig. Figure 2 and Fig. Figure 3), deterioration of accuracy for equations (Eq. (40)) and (Eq. (41)) occurs mainly for the heaviest macrostates, and is the most severe for the largest trajectory set. In our analysis of POPC trajectory sets, it seems that finer definitions of conformer give smaller $\Delta\delta$ terms. The observation seems to contradict our speculation on the scenario when misCSCG approaches the microscopic extreme. The consequence of too-fine conformers might be better understood from an alternative perspective with a thought experiment. Robustness of approximations in equations (Eq. (40)) and (Eq. (41)) corresponds to the near-perfect cancellation of change of intra-conformer entropy and change of enthalpy as reflected by equations (Eq. (39)) and (Eq. (42)), without sufficient number of complex and heterogeneous microstates within each conformer, it is hard to imagine how such EEC occur. Consistently, a simple Morse potential type of protein-ligand interaction model was found only able to exhibit weak EEC.⁴¹ This thought experiment suggests that the problem of too-fine conformers is likely to explicitly surface in a full quantum mechanical treatment of the system, which will be an important issue to be investigated further. Analysis of these two extremal scenarios suggests that to guarantee the robustness of approximations in equations (Eq. (40)) and (Eq. (41)), conformers on the one hand need to be sufficiently small to ensure uniformity, and on the other hand to be sufficiently large to allow sufficiently efficient counting and effective EEC. Simultaneous satisfaction of these two requirements is not guaranteed by any physical law. We speculate that for sufficiently simple systems, they might

become mutually exclusive. Theoretical and computational analysis on the essential complexity of the molecular system for satisfaction of these two requirements is an important part of our future work.

Practical challenges in application of misCSCG based free energy calculations

In present study, we utilized extensive MD trajectories to test the validity and potential applicability of the proposed methodology. The reason is that deconvoluting force fields and sampling errors from fundamental deficiencies of a given free energy method is a challenge beyond the scope of this study. However, the ultimate goal of developing the methodology is to use it for predictive studies. A few challenges need to be tackled. Firstly, there are two possible routes for calculating the number ratio of conformers ($\frac{N_{conf}^A}{N_{conf}^B}$) for end macrostates in equations (Eq. (37)) and (Eq. (38)). The first one is to obtain this ratio without knowing the values of both the numerator and the denominator, and converged sampling of two end macrostates, which is in many cases difficult or impractical, is essential for this purpose. The alternative is to calculate both the numerator and the denominator directly and then calculate the ratio. Since the number of conformers is usually astronomically large, some form of sampling is essential for obtaining them. As a matter of fact, importance sampling²⁴ in combination with sequential Monte Carlo⁴⁵ was demonstrated to be an efficient and reliable way of counting the number of conformers for fixed backbone and rigid side chain rotamers. However, to deal with complex solute-solvent systems, efficient strategies need to be developed for various types of molecules. Secondly, the method is in principle compatible with solvation models ranging from simple implicit ones to full explicit solvation. However, further detailed investigations are necessary for either selection of presently available solvation free energy methods or development of new ones. Thirdly, it is apparent that proper coarse-graining of configurational space is system specific. We demonstrated the feasibility of defining sufficiently fine and uniform conformers in POPC, extension to other types of molecules (e.g. proteins, nucleic acids, polysaccharides and solvents), which is essential to deal with multi-component heteroge-

neous molecular systems, is yet to be done. Our analysis of large scale POPC MD trajectories, while validated the robustness of equations (Eq. (40)) and (Eq. (41)) for this specific system on the one hand, presented the challenge of selecting convenient and efficient definitions of conformers for general molecular systems on the other hand. It is important to note that volume of configurational space increases exponentially with increasing molecular DOFs. Another critical factor needs to be considered is the roughness of free energy landscape (FEL). Should we have a flat FEL, it would have been extremely easy to define uniform conformers even macroscopically. Conversely, a more rugged FEL would engender the need for finer conformers to achieve certain uniformity, and larger trajectory sets are needed to genuinely reflect statistical weight distribution of a given set of conformers. It is intuitively expected that proteins and nucleic acids have rougher FEL than POPC does. Therefore, we expect that to carry out similar analysis as we did for POPC on typically sized proteins (~ 100 -residue or larger), dramatically (many orders of magnitude) larger MD trajectories are necessary. Unfortunately, generating such MD trajectory sets is beyond the computational resources we may obtain. Developing effective ways to validate misCSCG based end point free energy calculation for more complex molecular systems is an important part of our future work.

Differences between misCSCG and conventional coarse graining

Coarse graining is a widely utilized idea in computational analysis of complex molecular systems. The most widely utilized conventional strategy is to average out fast DOFs in a hierarchical way so as to reduce the number of explicit DOFs and accelerate simulations. Atomistic MD simulation is arguably the most successful coarse-graining strategy that has a strong theoretical foundation, the Born-Oppenheimer approximation. There has been very rich literature on further coarse-graining of molecular systems based on atomistic molecular mechanical models as discussed in many excellent review articles.^{46–51} Despite the great achievement of these coarse-grained studies, there has been a lack of general guidelines and accompanied controversies on the optimal way of coarse-graining. The fundamental start point of averaging out fast DOFs is a clear separation of time scales

for motions of explicit and implicit DOFs, which becomes a rather subjective and difficult decision when identification of the boundary between fast and slow motions is not as trivial as in the case of Born-Oppenheimer approximation. In reality, the assumed separation of time scales does not hold well in some cases. All DOF reduction based coarse graining strategies attempt to capture major valleys and barriers of the free energy landscape through a simplified configurational space, which excludes correlations between explicit and implicit DOFs. misCSCG is a different strategy where the full configurational space is constructed with correlations of all relevant DOFs explicitly considered, while coarse graining is effectively realized by taking defined conformers as basic units for probing the configurational space. More importantly, the resulting error is explicitly available from the $\Delta\delta$ terms in equations (Eq. (33) and Eq. (36)). It is noted that theoretical framework of misCSCG is not limited to any specific level of DOF representations, and therefore may be applied to the configurational space of any given conventional coarse-grained models. The widely utilized Markov State Model (MSM),^{52,53} which divides the configurational space of macromolecule into macroscopic states hierarchically, has been successfully utilized to unraveling many biomolecular processes. The goal of our misCSCG is to split the configurational space into sufficiently fine and uniform conformers, fundamentally different from that of MSM, where the major goal is to divide the configurational space into a small number of easily tractable and understandable partitions to explain biomolecular mechanisms related to major thermodynamically stable and metastable states (conformations).

Conclusion

In conclusion, we proposed a general end point free energy estimation method based on the postulate that for high dimensional complex molecular systems, it is possible to define sufficiently fine and uniform conformers through microscopic configurational space coarse graining. We further tested its validity and applicability in lipid POPC based on analysis of extensive MD trajectories. In this theory, it is found that when configurational space of a high dimensional system is divided

into sufficiently fine and uniform conformers, change of both free energy and conformational entropy are essentially determined by the number ratio of thermally accessible conformers in end macrostates. The theoretical framework provide a new perspective on the long standing enigma of entropy-enthalpy compensation, which is utilized to its full potential to accelerate free energy calculations. This method fully considers conformational variation in end macrostates and does not require overlapping of end macrostates in configurational space. The error term of the change of free energy, and error term (with its upper bound) of change of conformational entropy are explicitly available. These terms are practically convenient to construct since only end macrostates are involved. Tests with extensive MD trajectories of POPC suggest that proper misCSCG is practically feasible. The connection between misCSCG and EEC, between misCSCG and conventional DOF reduction based coarse graining are discussed. Important theoretically open questions and practical challenges for further development of misCSCG based end point free energy calculations are presented. The awkwardness of entropy definition present challenges for treatment of high dimensional continuous data in general. As application of entropy is not limited to physical systems, we believe that our idea of misCSCG is likely to be useful for efficient analysis of large high dimensional continuous data sets in other fields of research and applications.

Methods

To define conformers, we first take a given set of torsional DOFs (Fig. Figure 1), with each being divided into three torsional states ($0^\circ - 120^\circ$, $120^\circ - 240^\circ$ and $240^\circ - 360^\circ$), and utilize their unique combinations as conformers. Two structural states (i.e. snapshots) of a POPC molecule belong to the same conformer if and only if they share the same torsional state for each selected torsional DOF.

Trajectory sets TSA1, TSA2 and TSA3 are constructed from snapshots of POPC collected in simulation condition A in the supplementary table 2.²⁶ There were totally 34143653 snapshots, which collectively amount to a CTS of $\sim 6.15ms$ ($6.14585754ms$). Five subsets, with CTS being

$\sim 1.58ms$, $\sim 1.32ms$, $\sim 1.32ms$, $\sim 1.32ms$ and $\sim 0.66ms$ respectively, were available for this simulation condition. We take the first six trajectories out of the total 66 trajectories of the first subset as TSA1, which has a CTS of $142.56\mu s$. The first subset ($\sim 1.58ms$) was taken as TSA2, and the union of all subsets was taken as TSA3 ($\sim 6.15ms$). Trajectory sets TSB1a through TSB1f, TSB2a through TSB2e and TSB3 are constructed from snapshots of POPC collected in simulation condition B in the supplementary table 2.²⁶ There were 36724760 snapshots, which collectively amount to a CTS of $\sim 6.61ms$ ($6.6104568ms$). Five subsets, each including 56 trajectories with CTS being $\sim 1.32ms$, were available for this simulation condition and were taken as TSB2a through TSB2e. After trajectories of the first subset (TSB2a) were sorted according to file name, six equally-sized smaller sets denoted TSB1a through TSB1f were constructed from the first 36 trajectories, with each containing six consecutive trajectory files. The union of all subsets was taken as TSB3 ($\sim 6.61ms$).

To prepare macrostates, all snapshots in a given trajectory set were projected onto a selected backbone dihedral that was partitioned into 20 18° -windows, snapshots fall within each of which constitute an observed macrostate. Such projections were performed for 43 backbone dihedrals (Fig. Figure 1) and we have collectively 860 macrostates for each given combination of trajectory set and conformer definition. Apparently, macrostates based on the same dihedral angle do not overlap, while those based on different dihedral angles may overlap to different extent. To assign each snapshots to its belonging conformer and calculate N_{conf} for each constructed macrostates, torsional states for the selected torsional DOFs were encoded into bit vectors and the radix sort algorithm⁵⁴ was utilized.

Acknowledgement

This research was supported by National Natural Science Foundation of China under grant number 31270758, and by the Research fund for the doctoral program of higher education under grant number 20120061110019. Computational resources were partially supported by High Performance Computing Center of Jilin University, China. We thank DE Shaw Research for providing trajec-

tory sets. We thank Zhonghan Hu for insightful discussions.

References

- (1) Wehrl, A. *Reviews of Modern Physics* **1978**, 50, 221–260.
- (2) Chipot, C.; Pohorille, A. In *Free Energy Calculations, Theory and Applications in Chemistry and Biology*; Chipot, C., Pohorille, A., Eds.; Springer: Berlin Heidelberg New York, 2007.
- (3) Kirkwood, J. G. *Journal of Chemical Physics* **1935**, 3, 300–313.
- (4) Darve, E.; Pohorille, A. *The Journal of Chemical Physics* **2001**, 115, 9169.
- (5) Jarzynski, C. *Physical Review Letters* **1997**, 78, 2690–2693.
- (6) Hummer, G.; Szabo, a. *Proceedings of the National Academy of Sciences of the United States of America* **2001**, 98, 3658–61.
- (7) Goette, M.; Grubmüller, H. *Journal of Computational Chemistry* **2009**, 30, 447–456.
- (8) Ferrenberg, A. M.; Swendsen, R. H. *Physical Review Letters* **1989**, 63, 1195–1198.
- (9) Zwanzig, R. W. *The Journal of Chemical Physics* **1954**, 22, 1420.
- (10) Zwanzig, R. W. *The Journal of Chemical Physics* **1955**, 23, 1915.
- (11) Bash, P. a.; Singh, U. C.; Langridge, R.; Kollman, P. a. *Science (New York, N.Y.)* **1987**, 236, 564–8.
- (12) Lu, N.; Kofke, D. A. *The Journal of Chemical Physics* **1999**, 111.
- (13) Hansson, T.; Marelus, J.; Åqvist, J. *Journal of Computer-Aided Molecular Design* **1998**, 12, 27–35.
- (14) Kuhn, B.; Kollman, P. A. *Journal of Medicinal Chemistry* **2000**, 43, 3786–3791.

- (15) Meirovitch, H. *J. Chem. Phys.* **1999**, *111*, 7215–7224.
- (16) White, R. P.; Meirovitch, H. *The Journal of chemical physics* **2004**, *121*, 10889–10904.
- (17) Cheluvvaraja, S.; Meirovitch, H. *Journal of Chemical Physics* **2005**, *122*.
- (18) Cheluvvaraja, S.; Mihailescu, M.; Meirovitch, H. *The journal of physical chemistry. B* **2008**, *112*, 9512–22.
- (19) Meirovitch, H. *Journal of molecular recognition : JMR* **2010**, *23*, 153–72.
- (20) General, I. J.; Dragomirova, R.; Meirovitch, H. *Journal of chemical theory and computation* **2011**, *7*, 4196–4207.
- (21) Shannon, C. *The Bell System Technical Journal* **1948**, *27*, 379–423.
- (22) Kullback, S.; Leibler, R. A. *Ann. Math. Statist.* **1951**, *22*, 79–86.
- (23) Skilling, J. *Bayesian Analysis* **2006**, 833–860.
- (24) Zhang, J.; Liu, J. S. *PLoS computational biology* **2006**, *2*, e168.
- (25) Falconer, R. J.; Penkova, A.; Jelesarov, I.; Collins, B. M. *Journal of molecular recognition : JMR* **2010**, *23*, 395–413.
- (26) Dror, R. O.; Green, H. F.; Valant, C.; Borhani, D. W.; Valcourt, J. R.; Pan, A. C.; Arlow, D. H.; Canals, M.; Lane, J. R.; Rahmani, R.; Baell, J. B.; Sexton, P. M.; Christopoulos, A.; Shaw, D. E. *Nature* **2013**, *503*, 295–9.
- (27) Lumry, R.; Rajender, S. *Biopolymers* **1970**, *9*, 1125–227.
- (28) Imai, K.; Yonetani, T. *The Journal of biological chemistry* **1976**, *250*, 7093–7098.
- (29) Grunwald, E.; Steel, C. *Journal of the American Chemical Society* **1995**, *117*, 5687–5692.
- (30) Gallicchio, E.; Kubo, M. M.; Levy, R. M. *Journal of the American Chemical Society* **1998**, *120*, 4526–4527.

- (31) Liu, L.; Guo, Q.-x. *Chemical reviews* **2001**, *101*, 673–695.
- (32) Ford, D. M. *Journal of the American Chemical Society* **2005**, *127*, 16167–70.
- (33) Krishnamurthy, V. M.; Bohall, B. R.; Semetey, V.; Whitesides, G. M. *Journal of the American Chemical Society* **2006**, *128*, 5802–12.
- (34) Krishnamurthy, V. M.; Bohall, B. R.; Semetey, V.; Whitesides, G. M. *Journal of the American Chemical Society* **2006**, *128*, 5802–5812.
- (35) Starikov, E. B.; Nordin, B. *The journal of physical chemistry. B* **2007**, *111*, 14431–5.
- (36) Ward, J. M.; Gorenstein, N. M.; Tian, J.; Martin, S. F.; Post, C. B. *Journal of the American Chemical Society* **2010**, *132*, 11058–70.
- (37) Liu, G.; Gu, D.; Liu, H.; Ding, W.; Li, Z. *Journal of colloid and interface science* **2011**, *358*, 521–6.
- (38) Olsson, T. S. G.; Ladbury, J. E.; Pitt, W. R.; Williams, M. a. *Protein Science* **2011**, *20*, 1607–1618.
- (39) Ferrante, A.; Gorski, J. *Journal of molecular biology* **2012**, *417*, 454–67.
- (40) Starikov, E. B.; Nordin, B. *Chemical Physics Letters* **2012**, *538*, 118–120.
- (41) Chodera, J. D.; Mobley, D. L. *Annual review of biophysics* **2013**, *42*, 121–42.
- (42) Breiten, B.; Lockett, M. R.; Sherman, W.; Fujita, S.; Lange, H.; Bowers, C. M.; Heroux, A.; Whitesides, G. M. *Journal of American Chemical Society* **2013**, *135*, 15579–15584.
- (43) Tidemand, K. D.; Scho, C.; Holm, R.; Westh, P.; Peters, G. H. *The Journal of chemical physics* **2014**, *118*, 10889–10897.
- (44) Ahmad, M.; Helms, V.; Lengauer, T.; Kalinina, O. V. *Journal of Chemical Theory and Computation* **2015**, 150311103935007.

- (45) Zhang, J.; Chen, R.; Tang, C.; Liang, J. *The Journal of Chemical Physics* **2003**, *118*, 6102.
- (46) Suter, J. L.; Anderson, R. L.; Christopher Greenwell, H.; Coveney, P. V. *Journal of Materials Chemistry* **2009**, *19*, 2482.
- (47) Merchant, B. a.; Madura, J. D. *Annual Reports in Computational Chemistry*; Elsevier B.V., 2011; Vol. 7; pp 67–87.
- (48) Liwo, A.; He, Y.; Scheraga, H. a. *Physical Chemistry Chemical Physics* **2011**, *13*, 16890.
- (49) Takada, S. *Current Opinion in Structural Biology* **2012**, *22*, 130–137.
- (50) Brini, E.; Algaer, E. a.; Ganguly, P.; Li, C.; Rodríguez-Ropero, F.; van der Vegt, N. F. a. *Soft Matter* **2013**, *9*, 2108.
- (51) Noid, W. G. *Journal of Chemical Physics* **2013**, *139*.
- (52) Chodera, J. D.; Singhal, N.; Pande, V. S.; Dill, K. A.; Swope, W. C. *The Journal of Chemical Physics* **2007**, *126*, 155101.
- (53) Chodera, J. D.; Noñl, F. *Current Opinion in Structural Biology* **2014**, *25*, 135 – 144, Theory and simulation / Macromolecular machines.
- (54) Cormen, T. H.; Leiserson, C. E.; Rivest, R. L.; Stein., C. *Introduction to Algorithms*, 3rd ed.; MIT Press and McGraw-Hill, 2009.

Table 1: Details of the 43 torsions utilized in defining conformers for POPC.

Index	atom1	atom2	atom3	atom4	Index	atom1	atom2	atom3	atom4
1	C12	N	C11	C15	2	N	C11	C15	O1
3	C11	C15	O1	P1	4	C15	O1	P1	O2
5	O1	P1	O2	C1	6	P1	O2	C1	C2
7	O2	C1	C2	O21	8	C1	C2	O21	C21
9	C2	O21	C21	C22	10	O2	C1	C2	C3
11	C1	C2	C3	O31	12	C2	C3	O31	C31
13	C3	O31	C31	C32	14	O21	C21	C22	C23
15	C21	C22	C23	C24	16	C22	C23	C24	C25
17	C23	C24	C25	C26	18	C24	C25	C26	C27
19	C25	C26	C27	C28	20	C26	C27	C28	C29
21	C27	C28	C29	C210	22	C28	C29	C210	C211
23	C29	C210	C211	C212	24	C210	C211	C212	C213
25	C211	C212	C213	C214	26	C212	C213	C214	C215
27	C213	C214	C215	C216	28	C214	C215	C216	C217
29	C215	C216	C217	C218	30	O31	C31	C32	C33
31	C31	C32	C33	C34	32	C32	C33	C34	C35
33	C33	C34	C35	C36	34	C34	C35	C36	C37
35	C35	C36	C37	C38	36	C36	C37	C38	C39
37	C37	C38	C39	C310	38	C38	C39	C310	C311
39	C39	C310	C311	C312	40	C310	C311	C312	C313
41	C311	C312	C313	C314	42	C312	C313	C314	C315
43	C313	C314	C315	C316					

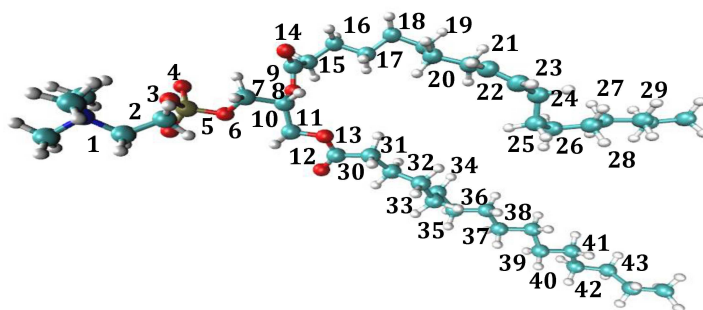


Figure 1: Ball and stick representation of POPC. Oxygen: red, hydrogen: white, carbon: cyan, phosphate: blue. The central bonds of 43 all-heavy-atom torsions (see Table Table 1 for details) utilized to define conformers are indicated with numbers. CONF1s are defined with all 43 torsions; CONF2s are defined by 28 torsions, which are {2,3,5,6,8,9,11,12,14,15,17,18,20,21,23,24,26,27,29,30,32,33,35,36,38,39,41,42}; CONF3s are defined by 22 odd numbered torsions and CONF4s are defined by 15 torsions that are excluded in the definition of CONF1.

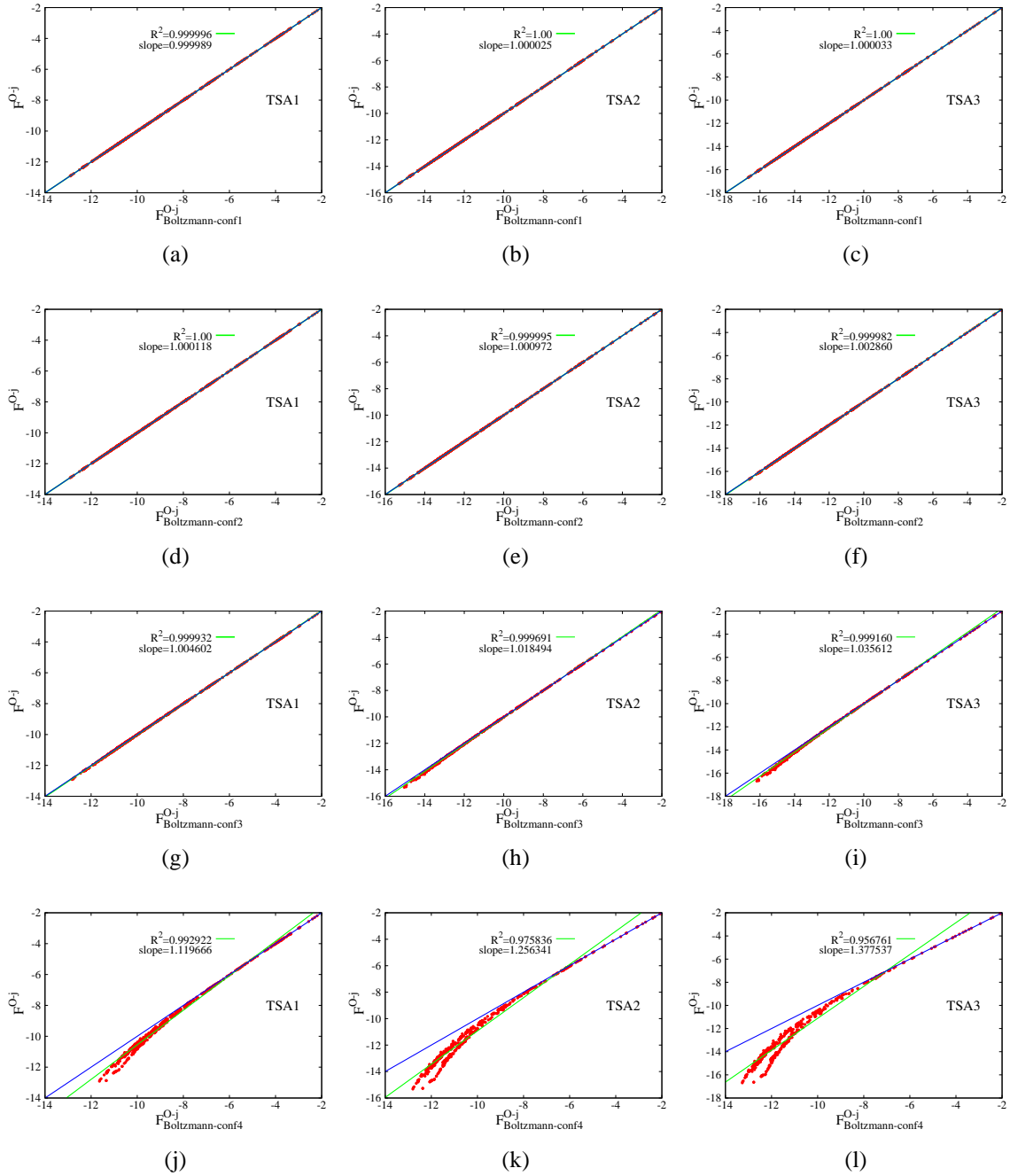


Figure 2: Free energy (in unit of $k_B T$) plots of POPC for 12 possible combinations of trajectory set and conformer definition. Three columns correspond to three given trajectory sets (TSA1 through TSA3) and four rows correspond to four definitions of conformers. Vertical axis is the relative free energy based on population of observed snapshots as shown in equation (Eq. (48)), horizontal axis is the relative free energy based on observed conformer counts for given conformer definitions as shown in equation (Eq. (49)). Blue lines represent scenarios where approximate equation (Eq. (40)) holds perfectly. Red dots are observed data points, each of which corresponds to a macrostate; green lines are best linear fit for the observed data with R^2 being the squared linear correlation coefficient. Specific trajectory sets is shown in lower-righter part of each plot.

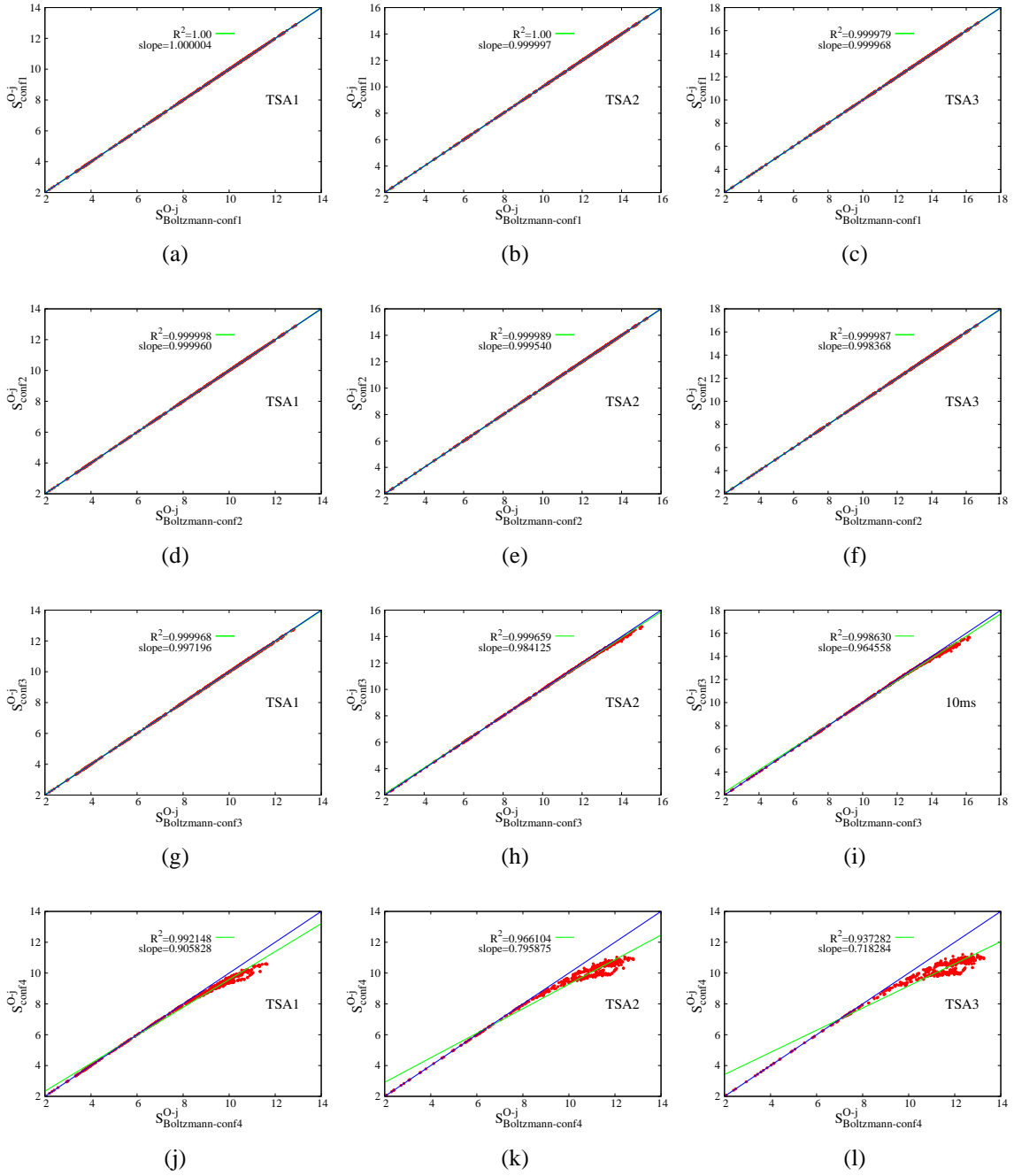


Figure 3: Conformational entropy (in unit of k_B) plots of POPC for 12 possible combinations of trajectory set and conformer definition. Three columns correspond to three given trajectory set and four rows correspond to four definitions of conformers (CONF1 through CONF4, indicated in axis labels). Vertical axis is the conformational entropy based on probabilities of observed conformers as shown in equation (Eq. (44)), horizontal axis is the conformational entropy based on observed conformer counts for given conformer definitions as shown in equation (Eq. (45)). Blue lines represent scenarios where approximate equation (Eq. (41)) holds perfectly. Red dots are observed data points, each of which corresponds to a macrostate; green lines are best linear fit for the observed data. The collective size of trajectory sets is shown in lower-righter part of each plot.

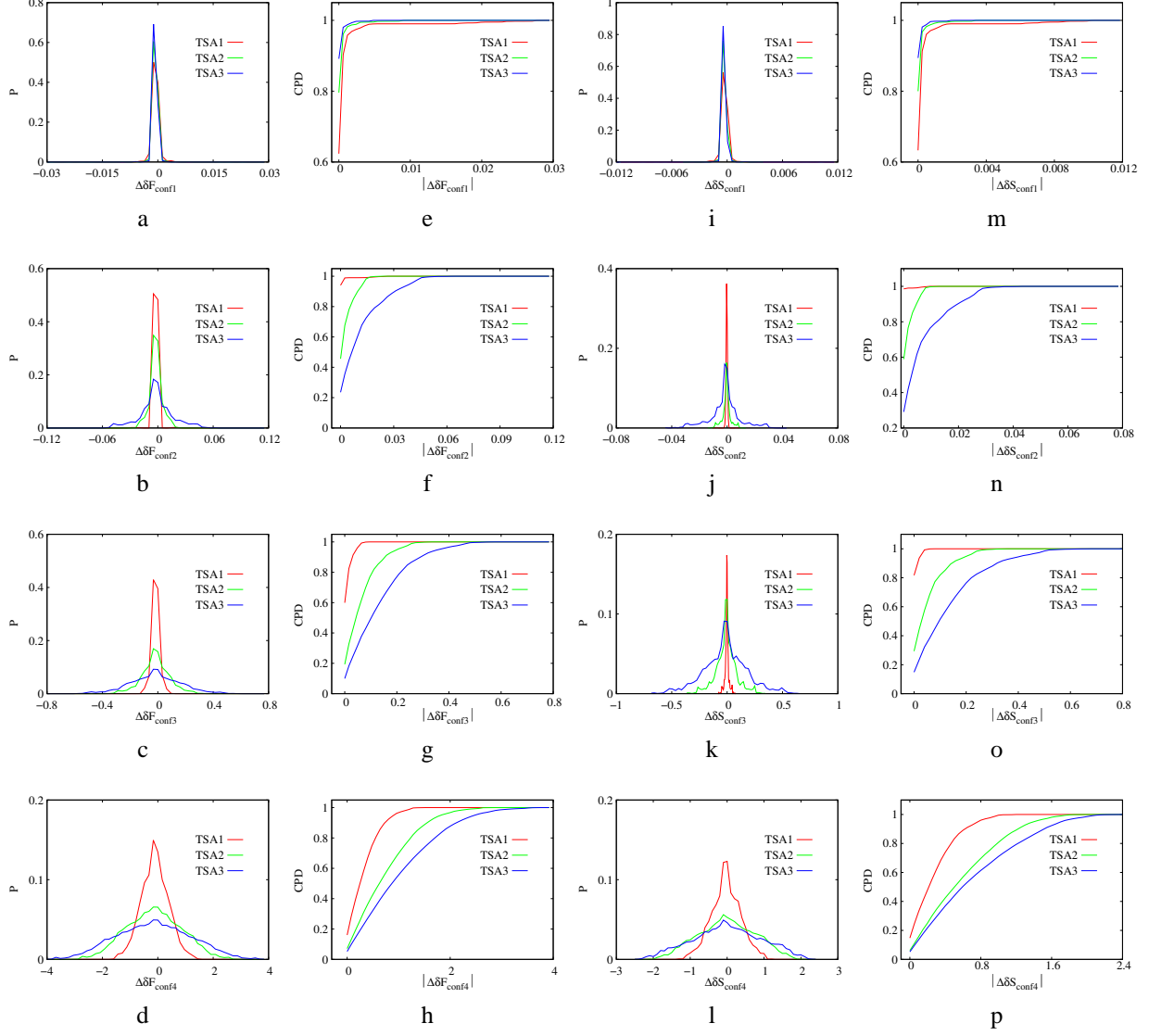


Figure 4: Observed $\Delta\delta F$ (in unit of $k_B T$) term in equation (Eq. (37)) and $\Delta\delta S_{conf}$ (in unit of k_B) term in equation (Eq. (38)) for POPC with the given conformer definitions. Different trajectory sets are represented by different line colors. (a-d) Distributions for $\Delta\delta F$ for CONF1 through CONF4; (e-h) CPD for absolute values of $\Delta\delta F$; (i-l) Distributions for $\Delta\delta S_{conf}$; (m-p) CPD for absolute values of $\Delta\delta S_{conf}$.

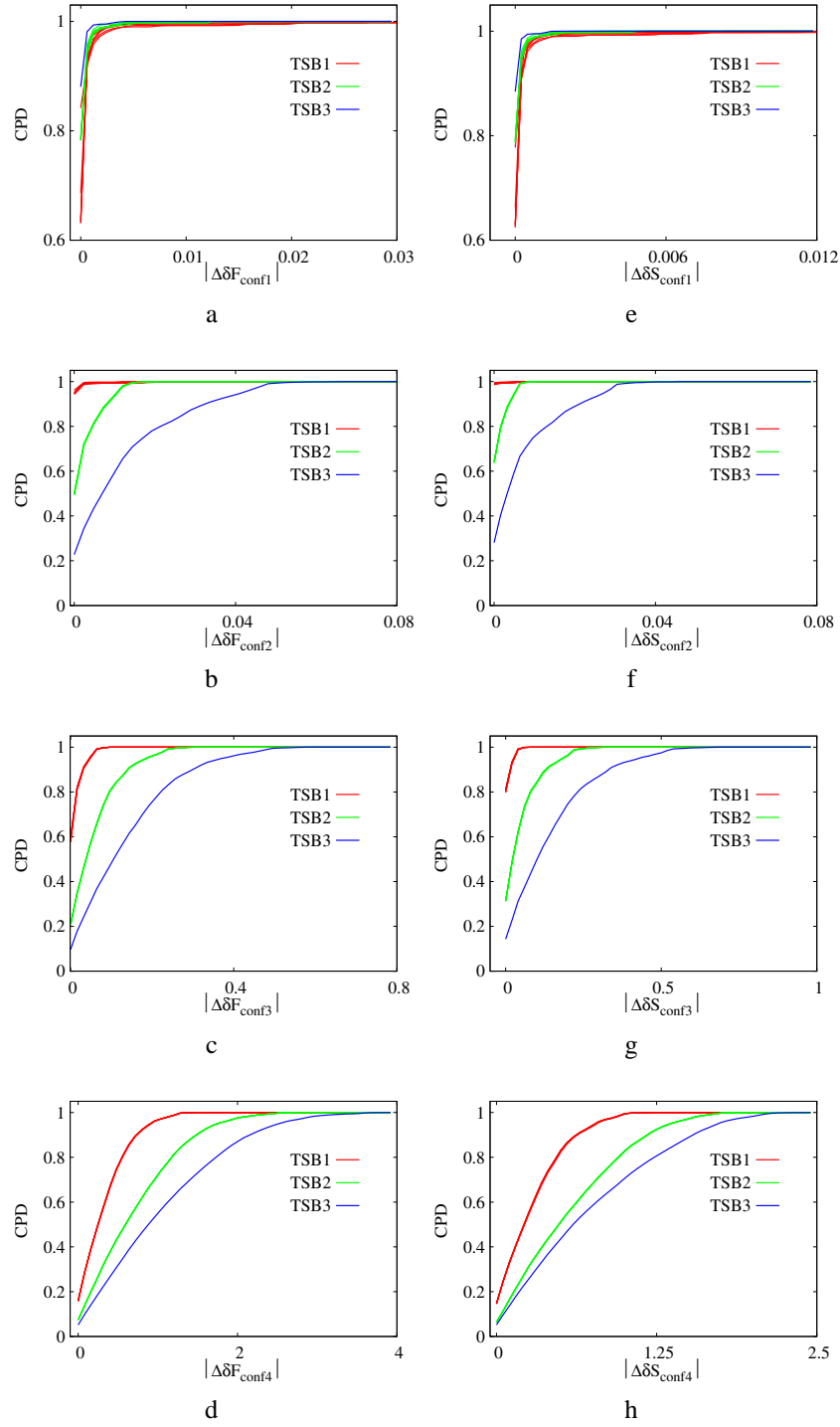


Figure 5: CPD of the absolute values of $\Delta\delta$ terms for CONF1 through CONF4 obtained from trajectory sets TSB1a through TSB1f, TSB2a through TSB2e and TSB3. Four rows correspond to CONF1 through CONF4. $\Delta\delta F$ (in unit of $k_B T$) is in the left column while $\Delta\delta S_{conf}$ (in unit of k_B) is in the right column. In each plot, there are six red lines corresponding to TSB1a through TSB1f, five green lines corresponding to TSB2a through TSB2e, and one blue line corresponds to TSB3. Same colored lines overlap in most of the plots.